



A Simple Method for Calculating the Shear Deformation of Reinforced Concrete Elements in the Elastic and Plastic Domains

Luisa Hdz-Gil¹ · Luisa María Gil-Martín¹ · Enrique Hernández-Montes¹

Received: 5 November 2022 / Revised: 3 June 2023 / Accepted: 23 June 2023
© The Author(s) 2023

Abstract

This paper proposes a simple method for calculating the shear deformation and the shear capacity of reinforced and prestressed concrete elements containing shear reinforcement. This new approach considers that, for large deformations, concrete elements follow compatibility conditions based on displacements of the composite material subjected to shearing forces. The result is a beam, inspired by the Timoshenko-Ehrenfest beam theory, which considers a new hypothesis regarding shearing deformation, informed by the behavior of the shear reinforcement. The new method is compared with previous approaches, allowing us to assess the technological advances of the new proposal. The new method is easy to implement and provides information about the shearing deformation (in the elastic and plastic domains) and the shearing capacity of concrete beam-column elements. A detailed example is developed, in which all the components of the shear deformation are evaluated, and the simplification of the new method is analyzed in comparison with other more comprehensive methods in the elastic domain.

Keywords Reinforced concrete elements · Compression field theories · Beam theories · Shear deformation · Deflexion of RC elements

1 Introduction

The study of the behavior of beam-column elements under shearing forces is still a challenge, [1–3].

The infinitesimal strain theory (also known as small deformation theory) is frequently adopted for civil engineering materials (concrete and steel) for the analysis of the deformation of structures, [4]. Nevertheless, for large deformations, this hypothesis may be unreliable, and other models or theories could be more accurate.

The use of displacement-based compatibility, as opposed to the infinitesimal strain theory, is still a topic of discussion. However, it has been demonstrated to be a

more realistic approach for the capacity design of reinforced concrete slabs [5–8].

However, the use of fiber elements for the calculation of the dynamic response of RC structures is very widespread, as in OpenSees [9], in which the deformation of fiber elements is based only on flexural deformation. The study of shear deformation and capacity when applied to structural elements is still a challenge [10], and the international community is concerned about finding a sound solution to calculate the shearing deformation and capacity of RC elements when using fiber elements. Recently, A fiber beam-column element that incorporates flexure-shear interaction for cyclic analysis of RC structures was recently proposed [11]. The element in [11] is based on the Timoshenko beam theory, in which the transverse shear deformation is assumed to be uniformly distributed along the section, and shear deformation is only held on by concrete (using the Modified Compression Field Theory, [12]).

A new simple method is proposed in this work for the shear deformation of beam-column elements, based on displacement compatibility. Section two presents an analysis of the well-known Timoshenko beam theory, which emphasizes what we have used in our approach.

✉ Enrique Hernández-Montes
emontes@ugr.es

Luisa Hdz-Gil
luisahernandez@correo.ugr.es

Luisa María Gil-Martín
mlgil@ugr.es

¹ E.T.S. Ingenieros de Caminos, Canales y Puertos, University of Granada, Campus Universitario de Fuentenueva, 18072 Granada, Spain

Section three introduces effective shear strain (γ_{eff}), a concept that enables the axial deformation of the shearing reinforcement to be converted into effective shear strain, and an interesting comparison of the new method with the work of Ueda et al. [13] is carried out. Section four is devoted to the compression field approach for calculating the angle of inclination of the strut. Finally, Section five combines tension stiffening of concrete with effective shear strain to formulate shear deformation, which is shown in a detailed example.

2 The Timoshenko-Ehrenfest Beam

The deflection calculation in the Euler–Bernoulli beam theory takes into account only the effect of the bending moment [14]. In section 39 of Timoshenko's book [14], titled 'Effect of Shearing Force on the Deflection of Beams,' the Timoshenko-Ehrenfest beam is introduced as an extension of the Euler–Bernoulli beam theory. This new theory considers the influence of shearing force in the deflection of structural elements. The two main hypotheses about the Timoshenko beam are:

- There is a mutual sliding of adjacent cross-sections along the length of the element, see Fig. 1a.
- As a result of the non-uniform distribution of the shearing stresses, the cross-sections, which are initially plane, become curved (see Fig. 1b taken from the original text).

Timoshenko considers that the cross-sections at the level of the centroid remain vertical and slide along one another, and that the slope of the deflection curve (dy_1/dx), only caused by shear, is equal to the shearing strain (γ) at the centroid of each cross-section.

With y_1 as the deflection caused by shear. The shearing strain may be expressed as:

$$\frac{dy_1}{dx} = \gamma = \frac{(\tau_{yx})_{y=0}}{G} = \frac{\alpha V}{AG} \quad (1)$$

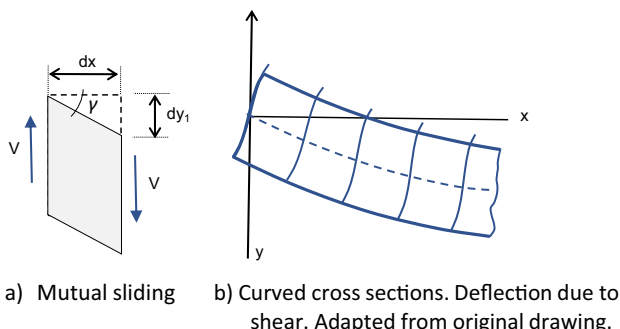


Fig. 1 Timoshenko-Ehrenfest beam. Adapted from [14]

where τ_{xy} is the shear stress, G is the shear modulus, V is the shear force, A is the cross-sectional area, and α is a factor with which the average shear stress (V/A) is multiplied to obtain the shear stress at the centroid of the cross section. An approximation for rectangular cross-sections is $\alpha = 3/2$ [14], for other cross-sections, Poisson's ratio is used, see [15].

If there is a continuous load on the beam (q), Eq. 1 can be differentiated, resulting in a curvature caused by shear given by:

$$\frac{d^2y_1}{dx^2} = \frac{\alpha}{AG} \frac{dV}{dx} = -\frac{\alpha}{AG} q \quad (2)$$

So, the total curvature of the beam (i.e. caused by both bending and shear) is:

$$\frac{d^2y}{dx^2} = -\frac{1}{EI_z} \left(M + \frac{\alpha EI_z}{AG} q \right) \quad (3)$$

With E as the modulus of elasticity, I_z as the principal moment of inertia in the z axis, and M as the bending moment in the same axis.

Equations (1) to (3) are taken from Timoshenko's book [14], and the original nomenclature has been used.

3 Effective Shear Strain

The approach proposed is inspired by the shear failure mode described in the American code (see Fig. 2a). Figure 2a is adapted from Figure R9.4.3.2a of §9.4 in the American code ACI-318 [16].

In this section, only shear deformation is going to be considered.

For large deformations, the shearing forces acting on reinforced concrete beam-column elements are mainly withstood by the transversal reinforcement (hoops, stirrups, and/or links). Figure 2b shows the portion of a beam with a crack, with θ as the angle of the crack. In Fig. 2b, only the blue stirrups are withstanding the shearing forces. Let δ_1 be the elongation of the stirrups induced by shear deformation.

In order to obtain an expression similar to Eq. 1, which can be differentiated, and subsequently introduced into the curvature expression, such as the expression that Timoshenko introduced in Eq. 3, an effective shear strain is defined (γ_{eff} , see Fig. 2c):

$$\gamma_{\text{eff}} = \frac{\delta_1}{z \cot \theta} \quad (4)$$

where z is the lever arm of the beam-column (see Fig. 2b). In Eq. 4, the shear reinforcement is assumed to be perpendicular to the axis of the element.

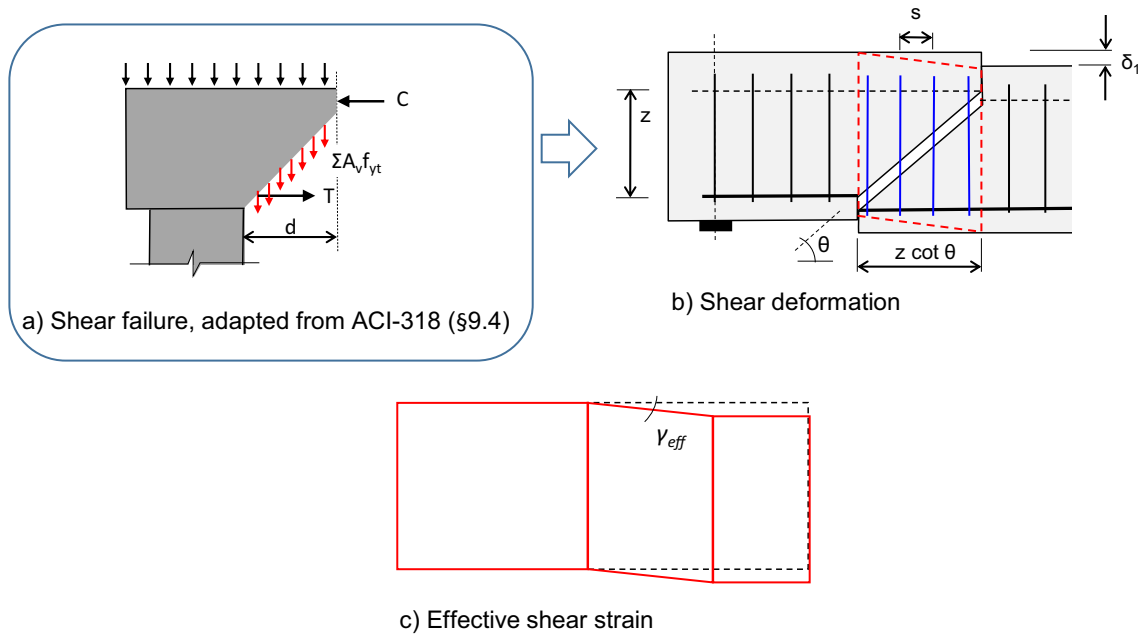


Fig. 2 Shear deformation and effective shear strain

Note that all the stirrups that contribute to the shearing deformation (in blue in Fig. 2b) have the same longitudinal strain (ϵ), given by:

$$\epsilon = \frac{\delta_1}{z} = \frac{\gamma_{eff} z \cot \theta}{z} = \gamma_{eff} \cot \theta \tag{5}$$

An embedded bar model is used here for the steel model. In doing so, the tension-stiffening behavior of the concrete surrounding each of the legs of the stirrups is considered for the stretching deformation.

Let $A_{c,eff}$ be the effective cross-sectional area of concrete in tension associated with each leg, A_{ϕ} is the cross-sectional area of each leg, and ϵ is the longitudinal strain of the leg. The effective area of concrete, $A_{c,eff}$, perpendicular to the bar, has been traditionally defined as the square area centered at the bar at a distance shorter than 7.5ϕ [17], with ϕ as the diameter of the bar. Recently, prEN1992 [18] has changed from 7.5 to 5.0. Maintaining the same capacity

results in an increase in the tensile stress of concrete due to the reduction in its effective area.

For a given value of ϵ , each leg of the transverse reinforcement contributes to the shear response with a force equal to (see Fig. 3):

$$A_{\phi} \sigma_{sv}(\epsilon) + A_{c,eff} \sigma_{ct}(\epsilon) \tag{6}$$

With σ_{sv} as the mean stress of the leg of the stirrup and σ_{ct} as the mean stress of the concrete. Both of these are measured along the length of the leg.

The contribution of concrete in the compression zone and the dowel action of the longitudinal reinforcement can be considered by adjusting the tension stiffening model for the concrete surrounding the legs, [19].

The angle of the crack (θ) can be obtained from linear elasticity by using compression field theories [12, 19–21]. These theories assume that the angle of the principal direction of compressive stress coincides with the angle of the principal direction of compressive strain [22]. The value of θ given by the compression field theories is validated in the next section by comparing it with two experimental results taken from the literature. Nevertheless, international regulations propose an approximate value of $\theta = 45$ degrees for beams with no axial load (e.g. ACI-318 [16]) while, θ equal to $0.5 \text{ArcTan}(2\tau/\sigma)$ can be used for beam-columns elements.

Note that the above formulation (Eqs. 4, 5, and 6) does not change if several cracks cross the stirrup, and so, the approach can be extended along the length of the beam-column element, Eq. 7.

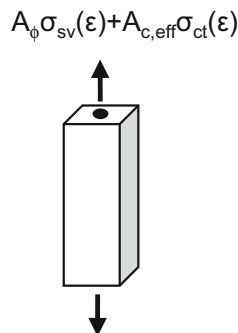


Fig. 3 Embedded bar model

$$\gamma_{eff} = \frac{\delta_1}{z \cot \theta} = \frac{dy_1}{dx} \quad (7)$$

Imposing vertical equilibrium in Fig. 4 and considering Eqs. 4, 5, and 6:

$$V(x) = \frac{z \cot \theta}{s} n_l (A_\phi \sigma_{sv} [\gamma_{eff} \cot \theta] + A_{c,eff} \sigma_{ct} [\gamma_{eff} \cot \theta]) \quad (8)$$

with n_l as the number of legs of each stirrup and s as the space between stirrups (see Fig. 4).

Once the shearing force diagram is known ($V(x)$), the value of the effective shear strain (γ_{eff}) as a function of x (i.e. $\gamma_{eff}(x)$) can be deduced from Eq. (8), and therefore the shear deformation can be obtained by numerical integration of $\gamma_{eff}(x)$ along the length of the beam-column element. The authors have used finite differences to do the numerical integration of $\gamma_{eff}(x)$ in the example presented in Sect. 5. The code is available upon reasonable request to the authors.

The theory presented here is of great practical interest because it enables the shear deformation (up to failure) of RC members to be obtained. Moreover, the formulation presented could easily be implemented in a new finite element.

3.1 Ueda's Approach

Ueda et al. [13] proposed a truss model for the study of shear deformation after shear cracking, Fig. 5a. In their approach, the deformation is separated in two: deformation caused by bending and deformation caused by shear. The deformation of the compression and tension chords is the flexural deformation, while the deformation of the struts and the ties is the shear deformation (δ_1), see Fig. 5b.

According to [13], the relation between shear strain (γ) and shear deformation (δ_1) is:

$$\gamma = \frac{\delta_1}{z(\cot \theta + \cot \alpha)} \quad (9)$$

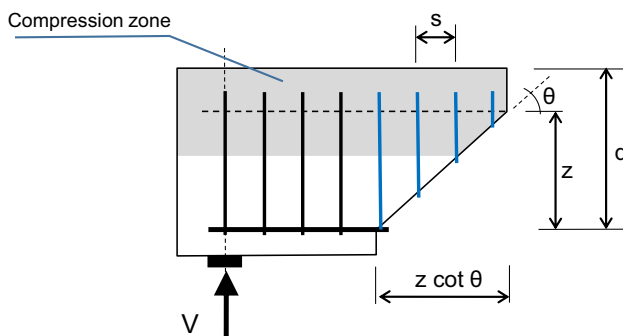


Fig. 4 Vertical equilibrium

which, for vertical stirrups ($\alpha = 90^\circ$) is the same as with Eq. 4. So, shear strain after shear cracking (γ) is the same as with the previously defined effective shear strain (γ_{eff}).

Based on very detailed experimental observations (laser speckle method), Ueda et al. [13] concluded that shear deformation before shear cracking can be neglected given that this type of deformation is usually much smaller than the flexural deformation.

Ueda et al. [13] proposed that shear strain after shear cracking is obtained as the summation of the shortening of the struts plus the elongation of the ties (Fig. 5b) as:

$$\gamma = \frac{V}{z(\cot \theta + \cot \alpha)^2} \left[\frac{1}{E_c b_w \sin^4 \theta} + \frac{s}{n_l (E_s A_\phi + E_c A_{c,eff}) \sin^3 \alpha} \right] \quad (10)$$

The first summand on the right side of the equality of Eq. 10 corresponds to the shortening of the strut (see Fig. 5b), and the second summand corresponds to the elongation of the tie. It can be proved that if the shortening of the strut is ignored in comparison to the elongation of the tie (i.e. if the first summand of Eq. 10 is not considered), then Eq. 10 is equal to Eq. 8 in the elastic range.

Ueda et al. [13] verified the goodness of fit of their method with an experimental campaign based on four point bending tests of beams in the post-shear cracking domain and in the elastic range.

Regarding the angle of the compressed strut, θ , in [13] this value was obtained from non-linear finite element analysis, and an expression to evaluate θ as a function of the shear span to depth ratio, and the tension and shear reinforcement ratios were proposed. So, in [13] the orientation of the struts (θ) in each specimen was a given data.

Other alternative methods can be used to obtain the value of θ , such as: CFT, MCFT [23], RA-STM[20], RFCT[24],¹

4 The Angle of the Compression Field

The Annex of this paper summarizes the compression field formulation needed to calculate the angle of the compression field (θ), as presented in prEN1992 [18].

Note that because in this case θ is unknown, both equilibrium and compatibility equations are necessary.

Two alternatives for the compatibility equations are developed in the Annex of this paper, and both of them are compared with two beams from the experimental test campaign shown in [25], where a typical four-point

¹ CFT stands for Compression Field Theory, MCFT stands for Modified Compression Field Theory, RA-STM stands for Rotating Angle Softened Truss Model, and RCFT stands for Refined Compression Field Theory.

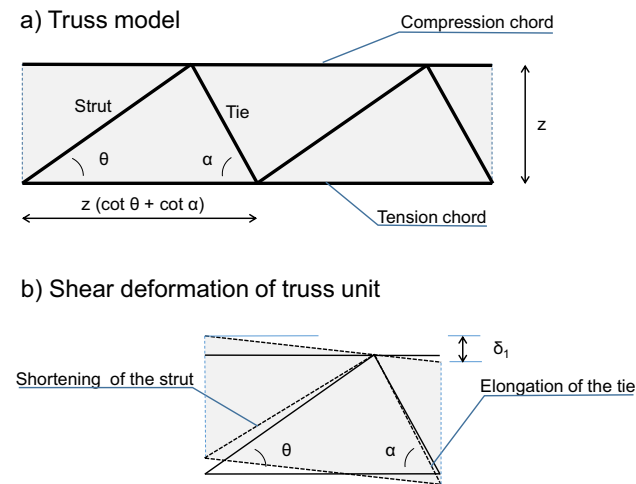


Fig. 5 Truss model for shear deformation. From [13]

bending scheme and setup were used (see Fig. 6). The two beams used for the comparison are the ST120 and the ST80, shown in Fig. 7.

The concrete compressive strength of the two beams tested was 28.5 MPa, and the yield strength of the transversal and longitudinal reinforcement was $f_{yt} = 310$ MPa and $f_{yl} = 550$ MPa, respectively. The longitudinal reinforcement layout is that shown in Fig. 6.

Beams ST120 and ST80 were shear reinforced with 5.5 diameter stirrups spaced at 120 mm and 80 mm, respectively. According to [25], the first cracks at the bottom appeared for $V = 35$ kN, inclined cracks appeared for $V = 50$ kN, and one big shear crack appeared for $V = 60$ kN in both specimens, see Fig. 7.

The cracking pattern in Fig. 7 shows that the inclination of the shear crack was 33° for the ST120 beam, and 36° for the ST80 beam.

The angles of inclination of the struts were theoretically obtained from the compression field developed in the Annex, and the best results are obtained when the small displacement hypothesis is used, and the compatibility equations are imposed at the bottom reinforcement. In this case, the inclination of the compression field obtained is 30° for the ST120 beam and 34° for the ST80 beam.

5 Example

The shear deformation of the beam in Fig. 8 is calculated and compared with the deformation caused by bending.

The example shown in Fig. 8 has been adapted from [26]. The values of the effective depth, the modulus of elasticity of concrete, and the steel yield stress are $d = 450$ mm, $E_{cm} = 30,500$ MPa and $f_y = 400$ MPa, respectively.

In the original example, the beam was subjected to a uniform load, q , that was equal to 16.9 kN/m. The shear demand, V_{Ed} , is calculated as a function of x , as shown in Fig. 9. At a distance of less than d from the face of the support, the shear demand is constant (EN 1992 [27], §6.2.1(8)).

The maximum short-term deflection for this load, calculated according to ACI-318[16], is 10.7 mm^2 while the value of the maximum short-term deflection calculated using the simplified method of EN 1992[27] is 11.2 mm^3 .

In this example, a bilinear tension stiffening model is adopted for concrete [28], see Fig. 10. The descending branch is defined by a certain point, ψf_{ctm} , of the ascending branch, ($\psi \leq 1$, and f_{ctm} is the mean axial tensile strength of concrete according to EN 1992 [27]), and the point that corresponds to the steel yield strain is (ϵ_y), for which the tension stiffening capacity is zero. Additionally, the model adopted presents a residual plateau that has been formulated as in [29]. In this example, the value of ψ is deduced in an indirect way from the minimum shear reinforcement ratio proposed by EN 1992 [27] (Expression 9.5N), which, when applied to this beam, leads to:

$$\begin{aligned} \frac{n_l A_\phi}{s b_w} &= 0.08 \frac{\sqrt{f_{ck}}}{f_y} \rightarrow \phi = 6.8 \text{ mm} \\ \psi f_{ctm} A_{c,eff \min} &= \psi f_{ctm} (50 + 7.5\phi)(2 \cdot 7.5\phi) \quad (11) \\ &= \frac{\pi \phi^2}{4} f_y \rightarrow \psi = 0.6 \end{aligned}$$

With b_w as the breadth of the beam ($= 300$ mm), $s = 240$ mm, $n_l = 2$, $f_{ck} = 25$ MPa, $f_{ctm} = 2.56$ MPa, and $A_\phi = \pi \phi^2 / 4$. The first of these equations leads to the minimum diameter of the stirrups that is needed to meet the minimum shear reinforcement requirement (resulting in $\phi = 6.8$ mm). In the second equation the maximum capacity of the concrete that surrounds a leg with $\phi = 6.8$ mm (whose effective concrete area is called $A_{c,eff \min}$, see Fig. 11) equals the tensile capacity of the leg (resulting in $\psi = 0.6$). The aim of Eq. (11) is to avoid sudden failure, and this objective is the reason why the provision of a minimum amount of shear reinforcement exists. Note that, as shown at a later point, this approximation is not relevant for large displacements, where the contribution of the concrete in tension is almost zero.

In the case of 10 mm diameter stirrups at 240 mm, the effective area of concrete proposed by prEN 1992 [18] is shown in Fig. 10.

Because the model adopted for steel lacks an apparent yield [20], both the bare bar model and the embedded bar

² This solution can be found in a video uploaded onto Youtube (https://www.youtube.com/watch?v=_YInm-fDRXs).

³ Likewise, the solution can be found in a video uploaded onto Youtube (<https://www.youtube.com/watch?v=BkXO6s2Ktwk>).

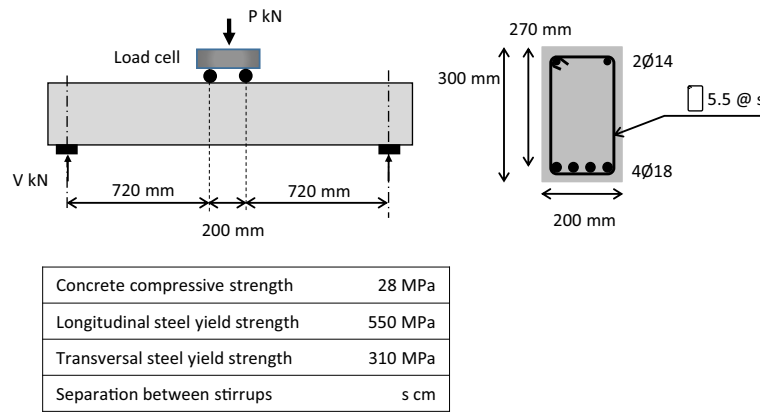


Fig. 6 Four-point bending test step up, adapted from [25]

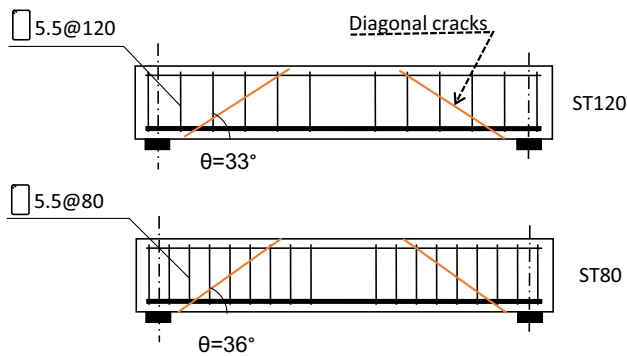


Fig. 7 Tested Beams ST120 and ST80, adapted from [25]

model are the same. So, the model of steel is defined by the modulus of elasticity ($E_s = 200,000$ MPa), the plastic modulus after yield ($E_s/100$), and the maximum strain (0.01). Additionally, it is assumed that the crack angle (θ) is 45 degrees (which is reasonable for a beam with no axial load).

From a theoretical point of view, Eq. 10, proposed by Ueda et al. [13] has two major drawbacks. The first one is that Eq. 10 assumes the linear behavior of the concrete in compression, which, according to EN1992, is true for stresses up to $0.4f_{cm}$ (for C25, $\sigma = 0.4f_{cm}$ corresponds to $\varepsilon = 0.000438$). According to Eqs. 19 and 20 in [13], the method described therein can be applied to determine the upper value of the shear force (with $z = 0.9d$):

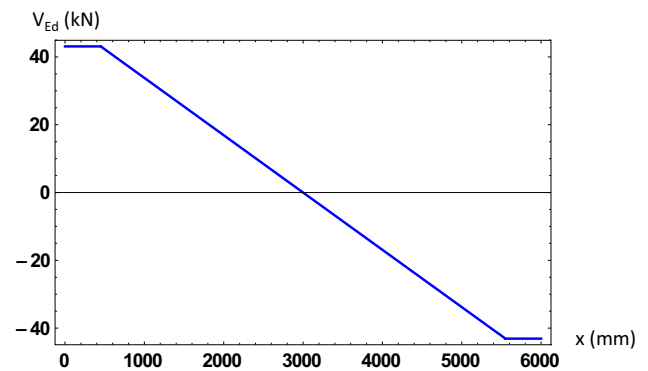
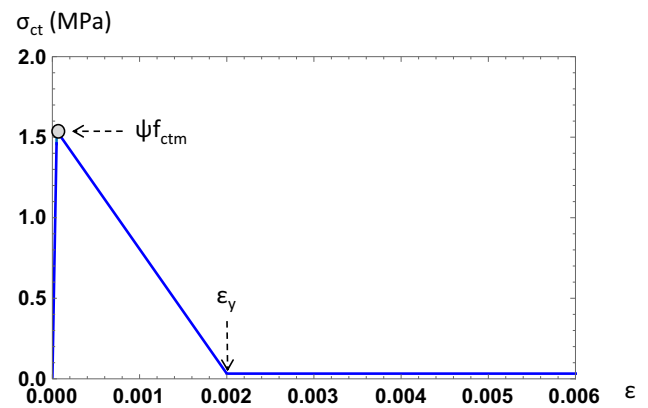

 Fig. 9 Shear demand in the beam in Fig. 8 for $q = 16.9$ kN/m


Fig. 10 Bilinear model for tension stiffening for concrete

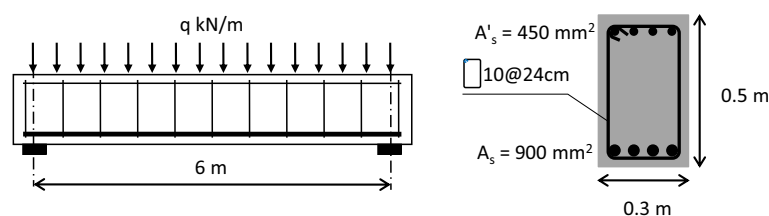


Fig. 8 Example of a reinforced concrete beam

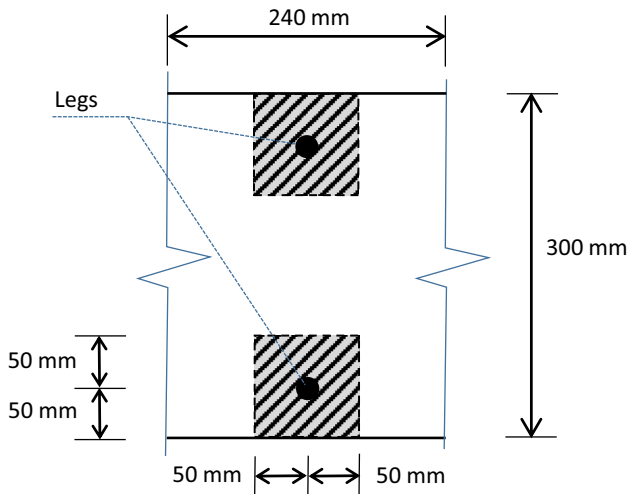


Fig. 11 Effective area of the concrete surrounding each leg, $A_{c,eff}$

$$V_{max} = 0.000438 E_{cm} b_w z \sin^2(\theta) (\cot(\theta) + \cot(\alpha)) = 812 \text{ kN}$$

The second drawback is that Eq. 10 does not consider either the tension stiffening of cracked concrete or the yielding of the steel. This limitation can be overcome by substituting the relation between V and γ given by the second summand of Eq. 10 with the relation given by Eq. 8, which considers both phenomena. Equation 8 summarizes the new method proposed in this paper.

Figure 12 (left) shows that before the cracking of concrete, the contribution of the shortening of the struts (dashed red line) to the shear strain is of the same order as that of the elongation of the ties (thick blue line). However, after cracking (Fig. 12 (right)), the contribution of the elongation of the ties to the shear strain (γ) grows significantly, as can be seen in this figure. For the value of the

strain corresponding to the yielding of the steel, the contribution of the shortening of the struts in the shear deformation of the beam is negligible.

In Fig. 12 (right), the two components on the right side of Eq. 8 and their summation are represented. The dashed blue line is the contribution of the steel, while the thin blue line is the contribution of concrete in tension (tension stiffening). The thick blue line is the summation of both contributions, steel and concrete. As can be observed, the tension stiffening effect can be considered to have disappeared when the steel yields.

Shear rotation (or shear strain) and shear deflection for the beam shown in Fig. 8, for values of q ranging from 17 to 47 kN/m, are represented in Fig. 13 (in this example, collapse happens at $q = 47.1$ kN/m). Due to symmetrical behavior only values from 0 to 3 m are shown in Fig. 13. It can be observed that the response is in the linear elastic range up to $q = 39$ kN/m (Fig. 13a) and in the plastic range for $q > 39$ kN/m. For $q = 17$ kN/m, shear deformation ($= 0.03$ mm) is negligible in comparison with bending deformation ($= 11$ mm). For $q = 39$ kN/m, the maximum deformation caused by shear is 0.088 mm at mid span, see Fig. 13a.

For load values over $q = 39$ kN/m, a major increment in both shear rotation and shear deflection occurs in the vicinity of the supports, see Figs. 13b and c. This increment is associated with the yielding of the legs of the stirrups located near the supports.

Figure 13 shows that the maximum shear deflection at mid span for $q = 40$ kN/m is 0.21 mm, while for $q = 47$ kN/m, it is 5.4 mm. The load increase and the corresponding increase in deflection show ductile behavior that is suitable for seismic engineering design.

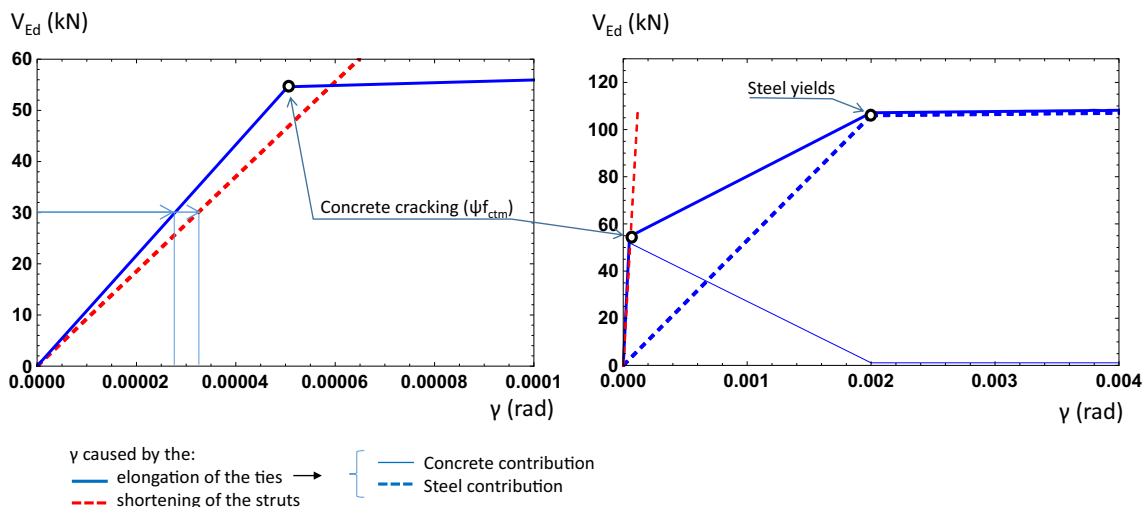


Fig. 12 Contribution of the shortening of the struts and the elongation of the ties to the shear strain

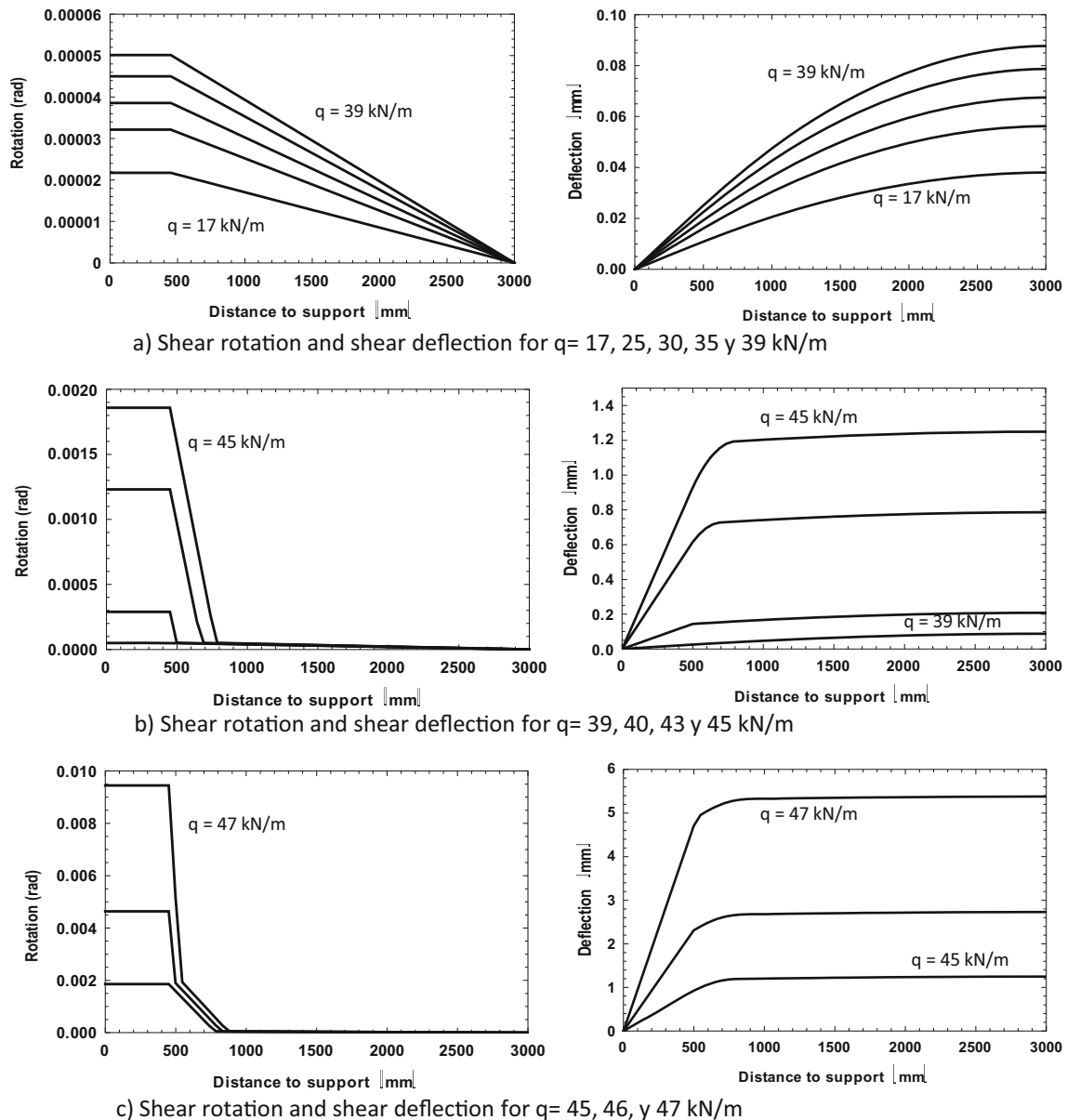


Fig. 13 Shear rotation and shear deflection in the beam for several values of the uniform load, q

6 Conclusions

A new approach for the calculation of the shear deformation of beam-column elements made of reinforced concrete is presented in this paper. The approach proposed, based on the Timoshenko-Ehrenfest beam, is easy to implement, and it is in line with what other authors have proposed. The method proposed for obtaining the shear deformation of a beam provides a solution to a widespread concern in the structural engineering community.

Based on the results obtained for a beam of regular dimensions, the following conclusions can be reached:

- In the linear range, shear deformation is very small (negligible) in comparison with bending deformation
- Shear deformation is significant near collapse
- Near collapse, the accuracy of the tension stiffening model adopted for concrete is irrelevant for the study of the shear deformation of the RC elements
- Compatibility conditions based on the concept of effective shear strain is a very sound alternative that can be used to study the shear deformation of reinforced concrete elements.

Annex. Compression Field Based on EN1992

Compression fields (prEN1992 §8.2.3(1)) is a useful approach for studying the post-cracking shear behavior of beam-column members.

When cracking in the principal tension direction happens, the beam starts to work as a truss structure in which the actions are withstood by a combination of diagonal compressive struts in the concrete and both longitudinal and transverse ties. These components form the reinforcement that can resist the tension forces.

The structure is not determined because the angle of the compression field is not known a priori. So, compatibility and material behavior equations also have to be considered in conjunction with equilibrium equations.

The problem is solved in continuum mechanics by considering smeared stresses and strains. Figure 14 shows the external and internal actions considered in the compression field.

Internal and external actions (forces and moments) in Fig. 14 have to be equivalent, so:

$$\begin{aligned}
 C \sin \theta &= V_{Ed} \Rightarrow C = \frac{V_{Ed}}{\sin \theta} \\
 \left. \begin{aligned}
 F_{cd} \frac{z}{2} + F_{td} \frac{z}{2} &= M_{Ed} \\
 F_{cd} - F_{tc} + \frac{V_{Ed}}{\sin \theta} \cos \theta &= N_{Ed}
 \end{aligned} \right\} \quad (A.1) \\
 \Rightarrow F_{td} &= \frac{M_{Ed}}{z} + \frac{1}{2}(V_{Ed} \cot \theta - N_{Ed}) \\
 F_{cd} &= \frac{M_{Ed}}{z} - \frac{1}{2}(V_{Ed} \cot \theta - N_{Ed})
 \end{aligned}$$

Figure 15 shows the equilibrium equations in the compression field are (see Fig. 15):

$$\sigma_c b_w z \cos \theta \sin \theta = V_{Ed} \quad (A.2)$$

$$A_{sv} \sigma_{sv} = \sigma_c b_w s (\sin \theta)^2 \quad (A.3)$$

$$A_{sx} \sigma_{sx} = \frac{M_{Ed}}{z} + \frac{1}{2}(V_{Ed} \cot \theta - N_{Ed}) \quad (A.4)$$

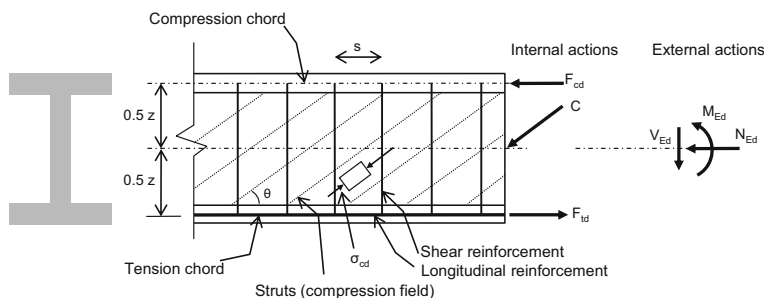


Fig. 14 Compression field of prEN1992 [18]. Notation for shear reinforced members

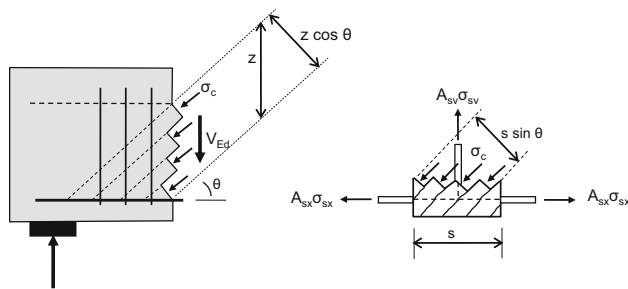


Fig. 15 Free-body diagrams

Equation A.2 is to the vertical equilibrium in the free body of Fig. 15-left. Equation A.3 is the vertical equilibrium in the free body of Fig. 15-right. Being $A_{sv} = n_1 A_{\phi}$, with n_1 as the number of legs of each of the stirrups, and A_{ϕ} as the cross-sectional area of the bar of the stirrup. It can be observed that as θ decreases, the required A_{sv} also decreases, since a greater number of stirrups act together to resist the shearing force. Equation A.4 is the equilibrium in the longitudinal tension reinforcement (i.e. $F_{td} = A_{sx} \sigma_{sx}$).

For given values of N_{Ed} , V_{Ed} and M_{Ed} , the equilibrium equations (A2, A3 and A4) can be solved as long as θ is known. In this case the unknowns are σ_c , σ_{sv} and σ_{sx} . On the contrary, if θ is unknown, compatibility equations are needed to solve the problem.

If the small displacement theory is used, new equations based on the infinitesimal strain tensor can be added as in CFT, MCFT [23], RA-STM [20], or RFCT [24]. See Fig. 16.

Based on the infinitesimal strain tensor, the following compatibility equations are obtained (Fig. 16):

$$\epsilon_1 = \epsilon_x + \epsilon_v - \epsilon_c \quad (A.5)$$

$$(\tan \theta)^2 = \frac{\epsilon_1 - \epsilon_v}{\epsilon_1 - \epsilon_x} \quad (A.6)$$

It is important to realize that the infinitesimal strain tensor can be used when the deformation of the solid body is very small, but for large deformations the infinitesimal strain tensor may not be appropriate.

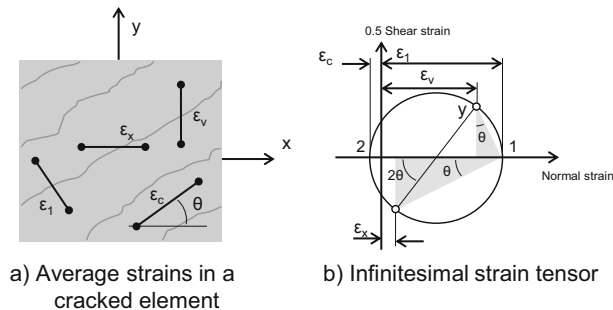


Fig. 16 Infinitesimal strain tensor

Equations for material behavior are needed to connect stresses and strains. Before plasticization, linear elastic behavior can be assumed for both concrete and steel:

$$\sigma_c = E_{cm}\varepsilon_c \quad (\text{A.7})$$

$$\sigma_{sv} = E_s\varepsilon_{sv} \quad (\text{A.8})$$

$$\sigma_{sx} = E_s\varepsilon_{sx} \quad (\text{A.9})$$

EN 1992 [18] formulates ε_x as the average strain of the bottom and top chords calculated at a cross-section that is no closer than $0.5z \cot \theta$ from a support or a concentrated load. For simplicity, we have formulated ε_x at the tension reinforcement (i.e. $\varepsilon_x = \varepsilon_{sx}$), which is a good representation of the behavior of the region close to the tension reinforcement.

Equations A.2–A.9 are a system of eight equations and eight unknowns (σ_2 , σ_{sv} , σ_{sx} , θ , ε_1 , ε_x , ε_c , ε_y), whose solutions are obtained numerically.

However, if instead of the small displacement theory, the large displacement theory is used, then compatibility is based on displacements, see Fig. 17. In this case, l_0 is the reference length used for the deduction of the compatibility equations. From Fig. 17:

$$l_x = \frac{l_0}{\sin \theta} \quad (\text{A.10})$$

$$l_y = \frac{l_0}{\cos \theta} \quad (\text{A.11})$$

Accordingly, the strains at the reinforcements in x and y directions are, respectively:

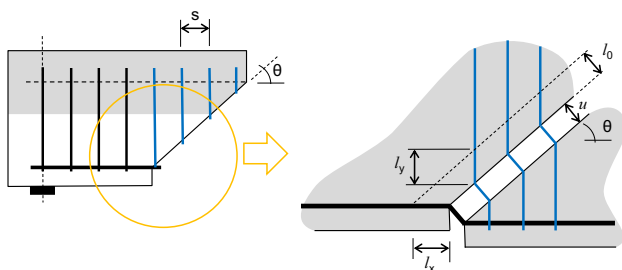


Fig. 17 Compatibility based on displacement

$$\varepsilon_x = \frac{u}{l_x} = \frac{u}{l_0/\sin \theta} = \varepsilon_1 \sin \theta \quad (\text{A.12})$$

$$\varepsilon_y = \frac{u}{l_y} = \frac{u}{l_0/\cos \theta} = \varepsilon_1 \cos \theta \quad (\text{A.13})$$

which are the compatibility equations.

So, if the large displacement theory is used, then Eqs. A.5 and A.6 have to be changed by A.12 and A.13.

Funding Funding for open access charge: Universidad de Granada/CBUA.

Data Availability The code developed for the example is available upon request to the authors.

Declarations

Conflict of Interest On behalf of all the authors, the corresponding author states that there is no conflict of interest.

Open Access This article is licensed under a Creative Commons Attribution 4.0 International License, which permits use, sharing, adaptation, distribution and reproduction in any medium or format, as long as you give appropriate credit to the original author(s) and the source, provide a link to the Creative Commons licence, and indicate if changes were made. The images or other third party material in this article are included in the article's Creative Commons licence, unless indicated otherwise in a credit line to the material. If material is not included in the article's Creative Commons licence and your intended use is not permitted by statutory regulation or exceeds the permitted use, you will need to obtain permission directly from the copyright holder. To view a copy of this licence, visit <http://creativecommons.org/licenses/by/4.0/>.

References

- Broujerdian V, Karimpour H, Alavikia S (2019) Predicting the shear behavior of reinforced concrete beams using non-linear fracture mechanics. *Int J Civ Eng* 17(5):597–605. <https://doi.org/10.1007/s40999-018-0336-6>
- Karaton M, Osmanlı ÖF, Gülşan ME (2021) Investigation of uncertainties in nonlinear seismic analysis of the reinforced concrete shear walls. *Int J Civ Eng* 19(3):301–318. <https://doi.org/10.1007/s40999-020-00567-8>
- Yang Z, Lei Y, Li G (2022) Experimental and finite element analysis of shear behavior of prestressed high-strength concrete piles. *Int J Civ Eng*. <https://doi.org/10.1007/s40999-022-00748-7>
- Ferreira AJM, Ribeiro MCS, Marques AT (2004) Analysis of hybrid beams composed of GFRP profiles and polymer concrete. *Int J Mech Mater Des* 1(2):143–155. <https://doi.org/10.1007/s10999-004-1493-0>
- Gil-Martín LM, Hernández-Montes E (2019) Closure to "Discussion on 'Strain compatibility in the strength design of RC slabs' by L.M. Gil-Martín, E. Hernández-Montes [Eng. Struct. 178 (2019) 423–435]. *Eng Struct* 200(109730):1–5. <https://doi.org/10.1016/j.engstruct.2018.10.045>
- Kaufmann W (2019) Discussion on 'Strain compatibility in the strength design of RC slabs' by L.M. Gil-Martín, E. Hernández-Montes [Eng. Struct. 178 (2019) 423–435]. *Eng Struct*

- 189(March):241–242. <https://doi.org/10.1016/j.engstruct.2019.03.073>
7. Gil-Martín LM, Hernández-Montes E (2021) Review of the reinforcement sizing in the strength design of reinforced concrete slabs. *Comput Concr* 27(3):211–223. <https://doi.org/10.12989/cac.2021.27.3.211>
 8. Gil-Martín LM, Hernández-Montes E (2019) Strain compatibility in the strength design of RC slabs. *Eng Struct*. <https://doi.org/10.1016/j.engstruct.2018.10.045>
 9. McKenna F, Fenves GL, Scott MH (2000) Open system for earthquake engineering simulation. University of California, Berkeley
 10. Bypour M, Kioumars M, Yekrangnia M (2021) Shear capacity prediction of stiffened steel plate shear walls (SSPSW) with openings using response surface method. *Eng Struct* 226(August 2020):111340. <https://doi.org/10.1016/j.engstruct.2020.111340>
 11. Feng D-C, Xu J (2018) An efficient fiber beam-column element considering flexure–shear interaction and anchorage bond-slip effect for cyclic analysis of RC structures. *Bull Earthq Eng* 16(11):5425–5452. <https://doi.org/10.1007/s10518-018-0392-y>
 12. Vecchio FJ, Collins MP, Vecchio FJ, Collins MP (1986) The modified compression-field theory for reinforced concrete elements subjected to shear. *ACI J* 83(2):219–231
 13. Ueda T, Sato Y, Ito T, Nishizono K (2002) Shear deformation of reinforced concrete beam. *Doboku Gakkai Ronbunshu* 2002(711):205–215. https://doi.org/10.2208/jscej.2002.711_205
 14. Timoshenko SP (1948) *Strength of materials (part I)*. Second Ed., New York
 15. Cowper G (1966) The shear coefficient in Timoshenko's beam theory. *J Appl Mech* 33:335–340
 16. ACI Comité 318 (2019) *Requisitos de Reglamento para Concreto Estructural (ACI 318S-19)*
 17. Bentz EC (2005) Explaining the riddle of tension stiffening models for shear panel experiments. *J Struct Eng* 131(9):1422–1425. [https://doi.org/10.1061/\(asce\)0733-9445\(2005\)131:9\(1422\)](https://doi.org/10.1061/(asce)0733-9445(2005)131:9(1422))
 18. prEN1992-1-1 (2023) *Eurocode 2: design of concrete structures—Part 1-1: General rules and rules for buildings, bridges and civil engineering structures EN 1992-1-1*. European Committee for Standardization, Brussels
 19. Gil-Martín LM, Hernández-Montes E, Aschheim M, Pantazopoulou SJ (2011) A simpler compression field theory for structural concrete. *Stud e Ric di Milano Sc di Spec Costr Cem Armato* 31:11–41
 20. Hsu T (1988) Softened truss model theory for shear and torsion. *ACI Struct J* 85(6):624–635
 21. Palermo M, Gil-Martín LM, Hernandez-Montes E, Aschheim M (2014) Refined compression field theory for plastered straw bale walls. *Constr Build Mater*. <https://doi.org/10.1016/j.conbuildmat.2014.02.004>
 22. Hernández-Díaz AM, Gil-Martín LM (2012) Analysis of the equal principal angles assumption in the shear design of reinforced concrete members. *Eng Struct* 42:95–105. <https://doi.org/10.1016/j.engstruct.2012.04.010>
 23. Collins MP, Mitchell D (1991) *Prestressed concrete structures*. Prentice Hall, New Jersey
 24. Gil-Martín LM, Hernández-Montes E, Aschheim MA and Pantazopoulou P (2009) Refinements to compression field theory, with application to wall-type structures. In *American Concrete Institute, ACI Special Publication*, no. 265 SP
 25. Karayannis CG, Chalioris CE (2013) Shear tests of reinforced concrete beams with continuous rectangular spiral reinforcement. *Constr Build Mater* 46:86–97. <https://doi.org/10.1016/j.conbuildmat.2013.04.023>
 26. CEB (1983) *CEB Design Manual on Cracking and deformations*. 1983. Comité Euro-International du Béton
 27. EN 1992-1-1 (2004) *Eurocode 2: Design of concrete structures—Part 1-1: General rules and rules for buildings*: European Committee for Standardisation
 28. Hdz-Gil L, Hernández-Montes E (2023) Linear concrete tension stiffening model for reinforced concrete elements. *Hormigón y Acero*. <https://doi.org/10.33586/hya.2023.3097>
 29. Lee SC, Cho JY, Vecchio FJ (2011) Model for post-yield tension stiffening and rebar rupture in concrete members. *Eng Struct* 33(5):1723–1733. <https://doi.org/10.1016/j.engstruct.2011.02.009>